Differential cross sections of the $^{12,13}C(p,p)^{12,13}C$ and $^{12,13}C(p,n)^{12,13}N$ reactions near 180°

Z. Yu,* R. E. Segel, and T.-Y. Tung†
Department of Physics and Astronomy, Northwestern University, Evanston, Illinois 60201

R. D. Bent, C. C. Foster, and J. Goodwin‡
Indiana University Cyclotron Facility and Physics Department, Bloomington, Indiana 47408

G. Hardie
Physics Department, Western Michigan University, Kalamazoo, Michigan 49008

J. Homolka
Physics Department, Technische Universität, München, Germany

(Received 25 September 1995)

The recoil detection method has been used to measure the differential cross sections at nucleon backward angles, 160°–180° (cm), for the $^{12,13}C(p,p)^{12,13}C$ and $^{12,13}C(p,n)^{12,13}N$ reactions at an incident proton energy of 200 MeV. These are the first reported data in this angular region. The elastic scattering cross sections show a shallow minimum at 180° and are about a factor of 15 larger than those predicted by optical model calculations using standard parameters. The (p,n) cross sections are lower than the (p,p), flat within the rather limited statistics, and about a factor of 5 greater than predicted. The backward-angle elastic scattering cross sections are selectively sensitive to the real central potential and can be brought into fairly good agreement with experiment without destroying the fit at more forward angles by greatly reducing both its depth and diffuseness. Adding a Majorana exchange term in the real central and spin orbit potential to a phenomenological potential that fits previously reported lower-angle ^{12}C elastic scattering data does not significantly alter these fits while introducing a peak at 180°.

PACS number(s): 25.40.Cm, 24.10.Ht, 25.40.Kv

I. INTRODUCTION

Performing distorted-wave Born approximation (DWBA) calculations using an optical potential has long been the accepted procedure for analyzing medium energy nucleon-nucleus elastic scattering. Impressive fits have been made to a wide variety of data and the optical model parameters thus found are used in distorted-wave impulse approximation (DWIA) calculations of inelastic scattering and other nuclear reactions. Meyer *et al.* [1] investigated $^{12}C(p,p)$ elastic scattering out to about 157° (cm) at 122, 160, and 200 MeV and at large angles found significant discrepancies between optical model calculations and experiment. When a standard optical model potential [2] is used the calculations give good fits from about 6° to about 130° except that the minimum observed at about 95° at all three energies is not reproduced. The fits in the 95° region can be improved considerably by using a double Woods-Saxon potential with a modified spin orbit term [1]. At all three energies the measured cross sections increase monotonically between 140° and 157° while the calculations, even with the modified potential, predict decreasing cross sections. By 157° the discrepancy is greater than an order of magnitude and apparently still increasing.

In order to further investigate this phenomenon the present experiment was undertaken in which elastic scattering of 200 MeV protons from ^{12}C and ^{13}C was measured between 160 and 180 degrees and, in addition, the differential cross sections for the $^{12}C(p,n)^{12}N$ and $^{13}C(p,n)^{13}N$ reactions were measured over the same angular range. The forward angle $^{12,13}C$ and $^{12,13}N$ recoils corresponding to backward emitted protons and neutrons were detected using the recoil detection system developed previously [3].

II. EXPERIMENT

A. Experimental setup

The experiment was performed at the Indiana University Cyclotron Facility (IUCF) where a 200 MeV proton beam with energy resolution $\Delta T/T<0.1\%$ passed through a 200 $\mu g/cm^2$ carbon target. Natural carbon (98.9% ^{12}C) was used for the ^{12}C targets while the ^{13}C targets were at least 99% ^{13}C. Target thickness tolerance was $\pm 10\%$. The recoils were analyzed by the QQSP spectrometer [4] which has a momentum range of $0.82 \leqslant p/p_0 \leqslant 1.37$, 0.1% momentum resolution, and ± 100 mrad angular acceptance in both the horizontal and vertical directions. However, in order to limit the influence of the out-of-bend-plane angle, an aperture was put at the entrance of the spectrometer restricting the angular acceptance to ± 50 mrad in the non-bend plane thus reducing the solid angle to 17.5 msr. In an ideal spectrometer ions of the same rigidity, $r=p/Q$, where p is the momentum and Q the atomic charge, are focused to the same distance, x, along the spectrometer's focal plane. However, computer raytrace simulations [4] have shown that the QQSP has significant aberrations which must be taken into account if the rigidity of the ions is to be accurately determined.

*Present address: Neptune Global Inc., Chicago, Illinois 60680.
†Present address: Physics Department, College of William and Mary, Williamsburg, Virginia 23185.
‡Present address: Fermilab, Batavia, Illinois 60510.

TABLE I. Coefficients for $r(x,\alpha)/r_0$, Eq. (1).

a_0	a_1	a_2	a_3	b_1	b_2	b_3	c_{11}
0.0056	0.0306	−0.0320	−0.341	0.950	0.233	−0.690	−0.0475

Recoils from the prolific [3] $^{12}C(p,\pi^+)^{13}C$ reaction were used to calibrate the spectrometer. From the kinematics the momentum locus $p(\theta)$ and therefore $r(\theta)/r_0$ were known. A thinner target, 46 μg/cm^2, was used in order to achieve better momentum resolution and, by varying the magnetic field, data were taken at several values of r_0. A series expansion was made for (r/r_0):

$$r(x,\alpha)/r_0 = 1 + a_0 + \sum_i^3 a_i(\Delta\alpha)^i + \sum_j^3 b_j(\Delta x)^j + c_{11}(\Delta\alpha)(\Delta x) \quad (1)$$

where

$$\Delta x = x - x_{\text{central ray}} = x - 0.21(\text{meter}), \quad (2)$$

$$\Delta\alpha = \alpha - \alpha_{\text{central ray}} = \alpha - 0.8048(\text{rad}) \quad (3)$$

Using the two-dimensional fitting code MINUIT [5] and starting with the (simpler) function found previously [4], $p/p_0 = b_1 x + a_1\alpha + c_1$, the coefficients given in Table I were determined.

After correcting for the (r/r_0) aberration, a 0.5% (r/r_0) momentum resolution was obtained. Although the spectrometer had a design momentum resolution of 0.1%, the 20 MeV ^{13}C recoils lost about 0.21 MeV in going through the 46 μg/cm^2 ^{12}C target limiting the resolution to $\Delta p/p = (1/2) \times (\Delta E/E) = 0.5\%$.

The experimental arrangement is shown in Fig. 1. In recoil experiments it is desirable that particles emerging at angles down to 0° be measured and the arrangement of Fig. 1 has been used in pion production experiments [3,6]. Because the recoils have less rigidity than the beam they are bent more and go through the spectrometer while the beam particles exit through the spectrometer's zero-degree exit port and into a Faraday cup. In the present experiment the C and N recoils had a considerably higher momentum than was encountered in previous experiments and were correspondingly more rigid. The spectrometer was, therefore, run at a higher magnetic field thus bending the beam so that it hit the walls of the exit port rather than cleanly going into the Faraday cup. In order to compensate for this extra bending a swing magnet was installed inside the zero-degree exit port. By varying the current in the swing magnet it was possible to show that there was a region of current over which the beam passed cleanly into the Faraday cup.

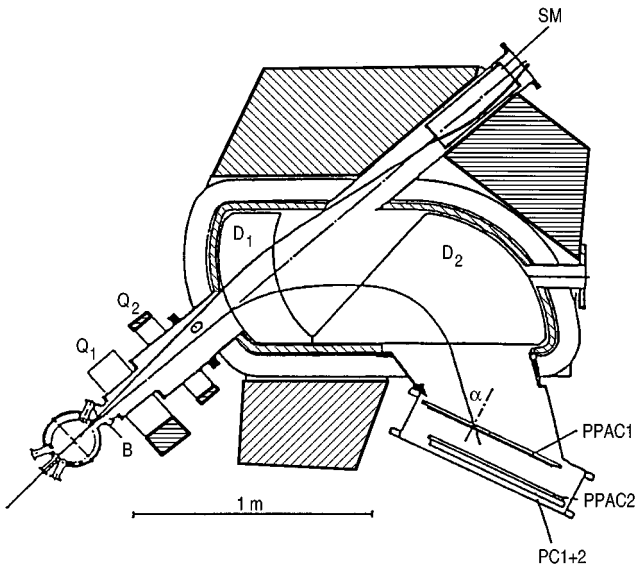

FIG. 1. Experimental setup. This setup is described briefly in the text and in more detail in Ref. [3] with the only change being the addition of the swing magnet, labeled SM, which bends the beam into the Faraday cup.

The detector stack, which was located at the focal plane of the QQSP, consisted of two identical parallel-plate avalanche counters (PPAC) and two identical proportional counters (PC). The details of the system have been described elsewhere [3]. Each of the two proportional counters measured the recoil's energy loss, ΔE. The average energy loss per unit length, $\Delta E/\Delta x$, was obtained by multiplying ΔE by $\cos(\alpha)/L$ where L is the thickness of the PC's active region. The arithmetic average of the two (dE/dx) signals was used in the data analysis.

A timing reference signal was taken from the cyclotron RF. After correcting for the time for the pulse to travel along the cathode foil, the recoil's time of arrival at the focal plane was obtained from the first PPAC. The time of flight between the two avalanche counters was used to determine a recoil's velocity with accuracy sufficient to identify the RF burst during which that recoil was created [3]. The time of arrival signal, combined with the RF signal, gave the recoil's time of flight through the spectrometer, t_1. Knowing the velocity and the rigidity, the ratio

$$(A/Q) = (1/m_{\text{nucleon}}) \times (p/Q)/v = (\text{const}) \times (r/r_0)/v \quad (4)$$

was determined. The combination of v and the energy loss in the proportional counters fixes the nuclear charge, Z. Knowing Z and (A/Q), with Q no larger than Z and with a limited number of possible Z, A combinations, it is usually possible to fix Z, A, and Q and thus identify a recoil and determine its momentum.

The velocity determination required a knowledge of the path length through the magnet and it was felt that the previous path-length calibration was inadequate. The new path length $\ell(x,\theta)$ calibration was performed using 11 strong A/Q peaks from berylium, boron, and carbon. Because most of these recoils were produced in reactions with more than two bodies in the final state, they tended to cover the entire focal plane. A series expansion was made for ℓ in terms of

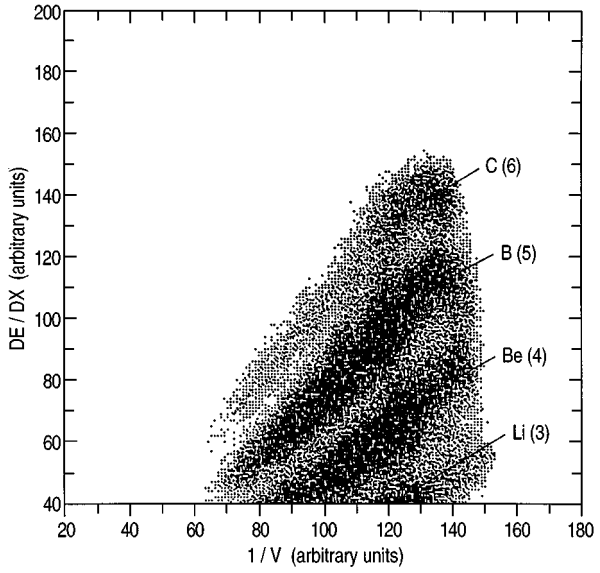

FIG. 2. Energy lost in the proportional counters, dE/dx, as a function of (ion velocity)$^{-1}$.

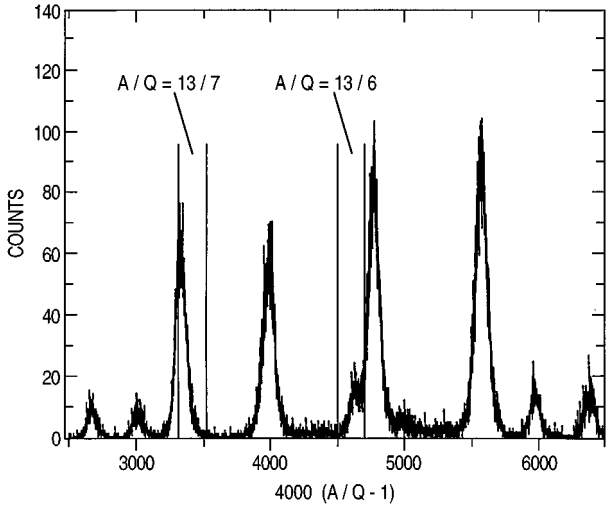

FIG. 3. Spectrum of A/Q taken with a ^{13}C target. The windows for recoils from elastic scattering, $A/Q=13/6$, and from (p,n) reactions, $A/Q=13/7$, are shown.

$\Delta\alpha$ and (r/r_0-1) and with this expansion, the calibrated (r/r_0), and the measured time of flight t_1

$$(A/Q)=(\text{const})\times(r/r_0)\times(t_1/\ell) \tag{5}$$

was calculated, and the sum of the squares of the difference between these calculated (A/Q)'s and the true (A/Q)'s was minimized. The calibrated ℓ polynomial had (r/r_0-1), $\Delta\alpha$, and cross terms all up to the power of 3.

Using the constants determined in the rigidity r/r_0 and pathlength ℓ calibrations the A/Q resolution was 0.8%. The differences between prior and present momenta and between prior [3,4] and present pathlengths are as big as 1.9% and 2.4%, respectively.

The total integrated beam was 30.0 milli-Coulombs on the natural carbon target and 29.9 milli-Coulombs on the ^{13}C target. The average beam current was about 600 nanoamps.

B. Data reduction

The time of flight between the two avalanche counters, t_2, and the pathlength between the two counters, l_{12}, as well as r/r_0 are used to obtain $(A/Q)_{t_2}$, where

$$(A/Q)_{t_2}=(\text{const})\times(r/r_0)\times t_2/l_{12}. \tag{6}$$

A two-dimensional histogram (A/Q) vs $(A/Q)_{t_2}$ is generated and a window placed on the histogram to select out events associated with the correct RF burst.

A two-dimensional dE/dx vs $1/v$ histogram is generated with the condition that events are within the RF window. Figure 2 shows such a histogram, which was taken with a ^{13}C target. In this histogram, $Z=2$, 3, 4, 5, and 6 groups are clearly delineated, although because of the suppressed zero the He ions are not observed in Fig. 2 and lithium is largely cut off. Because there are many fewer nitrogen events, the nitrogen group is difficult to see in the (dE/dx) vs $(1/v)$ histogram. Instead, the region of the nitrogen recoils is determined by calculating energy loss vs $(1/v)$ for $Z=3$, 4, 5, 6, and 7 using the code ENELOSS [7], and aligning the $Z=3$–6 curves, with common gain and offset, with the corresponding Z group and then placing the calculated $Z=7$ curve on the histogram. A window is then placed around this curve, as well as around the $Z=6$ group.

An A/Q histogram was generated with the RF window condition and a Z window condition. Figure 3 shows such a histogram from a ^{13}C target. The $A/Q=13/6$ of $^{13}C^{6+}$ differs by only 1.5% from the larger $A/Q=11/5$ of $^{11}C^{5+}$ and could not be completely separated from it. However, as is shown below, most of the $^{11}C^{5+}$ ions are in the low rigidity regions and are not a significant source of background in the region of the ^{13}C elastic scattering recoils. The 13/7 peak from ^{13}N is only 1.3% away from the much stronger 11/6 peak from ^{11}C and is therefore not discernible in Fig. 3. However, almost all of the C was eliminated when the Z cut was applied. The (p,N) recoils were isolated by placing windows around 13/6 and 13/7 for the ^{13}C target and 12/6 and 12/7 for the natural carbon target.

Two-dimensional histograms of α vs x are generated for events that satisfy the Z, A/Q and RF window conditions. Figures 4 and 5 show the histograms for $^{12}C^{6+}$ and $^{12}N^{7+}$, respectively, from the natural carbon target while Figs. 6 and 7 are for $^{13}C^{6+}$ and $^{13}N^{7+}$ from the ^{13}C target. Over the system's range of angular acceptance the kinematic locus for these (p,N) reactions is a nearly vertical line in θ vs rigidity. However, the spectrometer's aberrations distort this locus into having somewhat of an ''S'' shape. When the aberrations are taken into account, the data fall along the kinematic loci, as is illustrated in Fig. 8 where rigidity vs θ for recoils from several reactions in the ^{12}C target are compared to their respective kinematic ellipses. The (p,π^+) recoils had a greater momentum spread because they are of lower energy than the (p,N) recoils and therefore lost more energy in passing through the target.

For both C(p,p) reactions it was possible to leave the nucleus in an excited state while for both ^{12}N and ^{13}N only the ground state is particle stable. The only particle stable

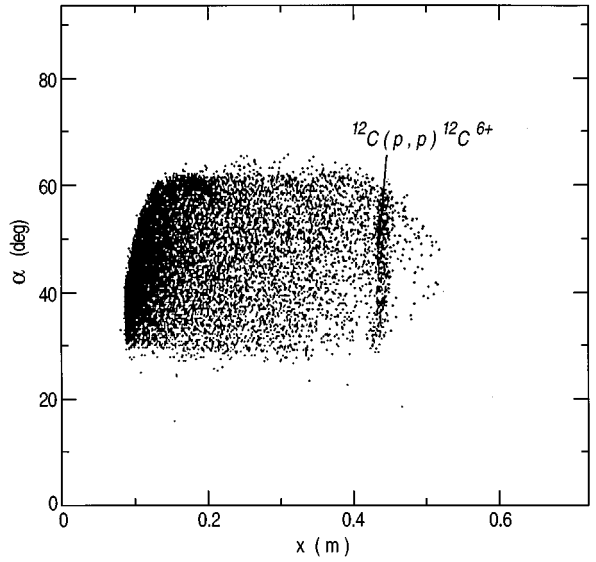

FIG. 4. Scatter plot of position along the focal plane (x) vs angle relative to the focal plane (α) of the events from a ^{12}C target with windows on $Z=6$ and $A/Q=2$ ($^{12}C^{6+}$). The vertical band at $x\approx 0.43$ contains the fully stripped recoils from elastic scattering. Most of the background is believed to be due to $^{10}C^{5+}$.

^{12}C excited state is at 4.44 MeV although the 15.11 MeV state also decays primarily by gamma emission. The kinematic locus for scattering to the 4.44 MeV state is also shown in Fig. 8 and it can be seen that most of the recoils appear to be from elastic scattering. Furthermore, DWIA calculations predict that the cross section to the ground state is about a factor of 20 greater than that to the first excited state. Combining the experimental and theoretical evidence, we conclude that the inelastic scattering contamination was less than 20%. Similar experimental and theoretical evidence lead us to the conclusion that most of the ^{13}C recoils from the

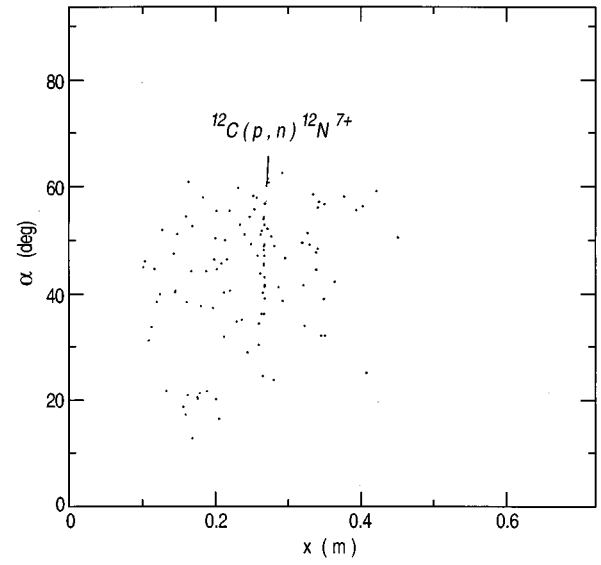

FIG. 5. Scatter plot of x vs α of the events from a ^{12}C target with windows on $Z=7$ and $A/Q=12/7$ ($^{12}N^{7+}$).

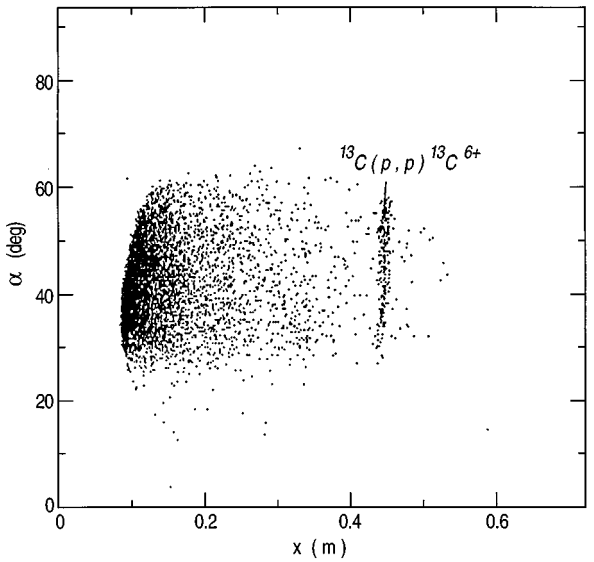

FIG. 6. Scatter plot of x vs α of the events from a ^{13}C target with windows on $Z=6$ and $A/Q=13/6$ ($^{13}C^{6+}$).

^{13}C target were from elastic scattering even though the 3.09, 3.68, and 3.85 MeV states are also particle stable.

Although reactions in which a single neutron or proton is emitted nearly opposite to the incoming beam direction comprise only about 10^{-6} of the total number of events they tend to stand out because of their high momentum transfer; the recoils of interest in the present experiment had momenta $\simeq$1200 MeV/c. When carbon and nitrogen recoils are being sought the Z window effectively eliminates everything below boron which, in turn, requires A to be at least equal to 8 with most of the boron likely to be either ^{10}B or ^{11}B (^{9}B is not particle stable). For $A=10$ nuclei the velocity window would allow only recoils with momenta greater than 560 MeV/c to be recorded. A similar threshold comes about because the

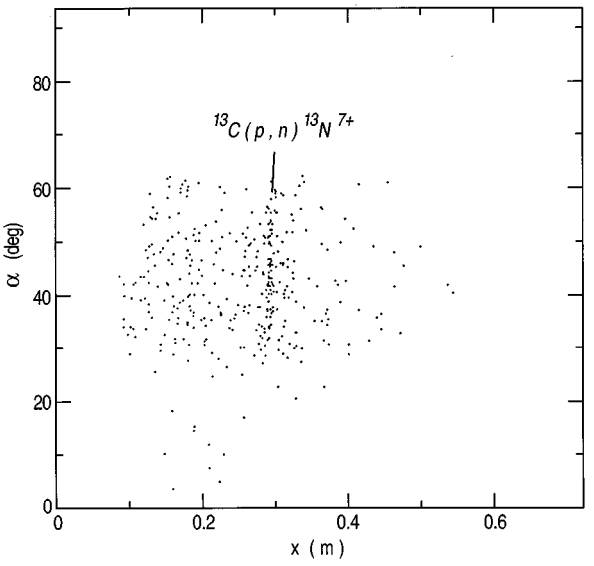

FIG. 7. Scatter plot of x vs α of the events from a ^{13}C target with windows on $Z=7$ and $A/Q=13/7$ ($^{13}N^{7+}$).

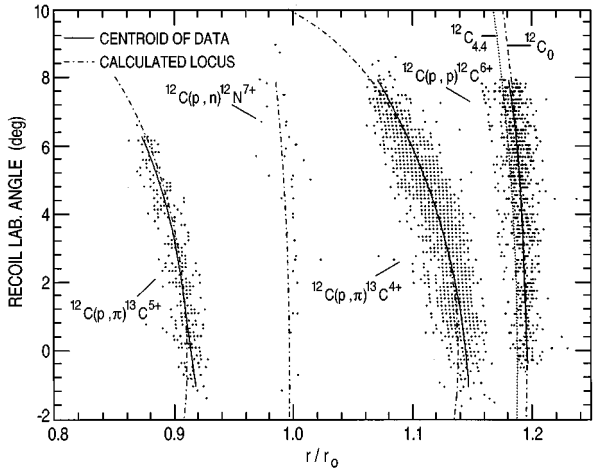

FIG. 8. Portions of rigidity vs emission angle histograms showing the recoils from various two-body final state reactions from $^{12}C+p$. Corrections have been made for the spectrograph's aberrations as described in the text. The dot-dash lines are the calculated loci and the solid lines the centroids of the data. For the ^{12}C recoils the dot-dash line is the calculated locus for elastic scattering and the dotted line that for scattering to the 4.44 MeV first excited state.

spectrometer would only accept particles with rigidities (p/Q) between about 134 and 224 MeV/c. Because the Z and v windows put an effective lower limit on Q of 3, this again led to only rather high momentum particles being accepted by the system.

In order to determine the background, a window is placed around each recoil group in the x-α histograms. The window is then moved, parallel to the x axis, to either side of the group for a distance just great enough to avoid overlap with the recoils of interest. Events within the recoil window and the two background windows in the x-α histogram are projected onto the α axis thus yielding a one-dimensional α distribution for both the region of interest and the background regions. The two background distributions are averaged to background$_{\text{average}}$ leading to:

$$\text{yield}=(\text{events}-\text{background}_{\text{average}}) \pm \sqrt{\text{events}+0.5\times\text{background}_{\text{average}}} \quad (7)$$

The cross sections at backward angles for the $^{12,13}C(p,p)$ and $^{12,13}C(p,n)$ reactions are as small as 10^{-7} mb/sr, while the total ion production cross section is about 10^{-1} mb/sr. Thus the system had to be selective enough to isolate the one in a million events that are of interest.

Part of the background can be attributed to the fact that only A/Q and Z are determined and that is not always sufficient to uniquely fix A. In particular, the $A/Q=2$ window cannot separate $^{12}C^{6+}$ from $^{10}C^{5+}$ and because the $^{10}C^{5+}$ ions are not from a two-body final state reaction they cover the entire x-α plane, although they are concentrated in the low rigidity region. As can be seen in Fig. 4, the $^{12}C^{6+}$ recoils from elastic scattering stand out clearly but there is a significant background which must be subtracted. As noted above, there is some $^{11}C^{5+}$ contamination in the $^{13}C^{6+}$ x-α histogram (Fig. 6) but it is concentrated at low rigidity and does not severely impact the region of the elastic scattering recoils. The $^{13}N^{7+}$ histogram may contain some $^{11}C^{6+}$ background because the Z separation is not complete and the A/Q values are only slightly different.

TABLE II. Signal/background ratios.

Reaction	$^{12}C(p,p)$	$^{13}C(p,p)$	$^{12}C(p,n)$	$^{13}C(p,n)$
Signal/background ratio	3.5	12.8	4.0	1.9

In addition to the background from spallation reactions, there may have been background from the beam being scraped as it passed through the mouth of the spectrometer. The signal to background ratios for all four reactions are given in Table II.

Only the fully stripped recoils are accepted and therefore a correction has to be made for the fraction that were in this atomic charge state. There have been several calculations of charge-state distributions [8–10] and at some energies they differ substantially. However, in the present work the ions of interest have enough energy so that most of the them ($>$85%) are fully stripped and the calculated charge-state populations differ by less than 10%. From the $^{12}C(p,\pi^+)^{13}C$ data that was taken while setting up the present experiment [11] it appears that the most recent calculation [10] best fits the charge-state populations observed for recoils from this reaction and therefore the population tables given in Ref. [10] were used in determining the cross sections.

The estimated systematic errors are listed in Table III. The effective solid angle of the QQSP spectrometer has never been measured to better than 10% [4]. The target thicknesses are deduced by measurements of weight and total target area and typically determine the thickness to better than $\pm$6%.

For the elastic scattering reactions there is an additional 10% uncertainty because of possible contamination from inelastic scattering. There is another additional 10% systematic error in the $^{12}C(p,p)$ cross sections due to the background subtraction, because for this reaction the background was relatively large and varied rapidly across the focal plane. These systematic errors are uncorrelated and therefore in the worst case, $^{12}C(p,p)$, amount to no more than 20%.

C. Experimental results

The methods described in the last section were used to obtain the yields as a function of α, and from these the center-of-mass differential cross sections were obtained. The results are shown in Figs. 9–12. Previously reported data on these reactions as well as DWIA calculations are also shown. The fact that the $^{12}C(p,p)^{12}C$ cross sections found here match on well to the results of Meyer *et al.* [1] lends support

TABLE III. Systematic errors.

Solid angle	10.0%
Target thickness	6.0%
Target impurity	1.1%
Beam integration	5.0%
Charge state population	5.0%
Total	13.7%

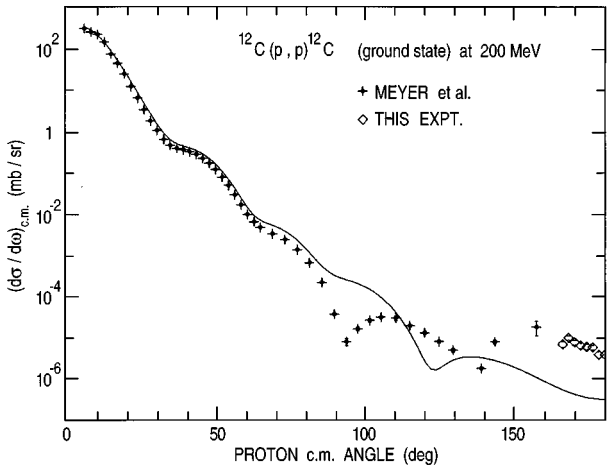

FIG. 9. Prior and present measurements and a DWIA calculation of the $^{12}C(p,p)^{12}C$ elastic scattering differential cross sections at 200 MeV. The DWIA calculation was done using the standard parameters. The crosses are from Ref. [1] and the diamonds the present work. Except for the point at 157° the errors are always smaller that the size of the symbols.

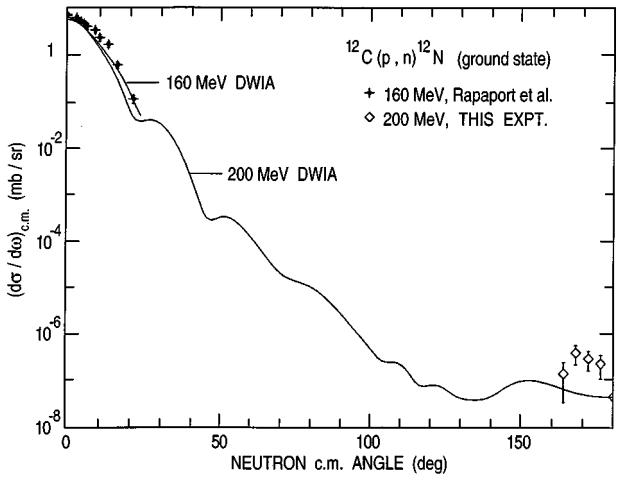

FIG. 11. Prior and present measurements and DWIA calculations of $^{12}C(p,n)^{12}N$ differential cross sections. The crosses are from Ref. [16] at 160 MeV and the diamonds the present work.

to the contention that the inelastic scattering contribution is small. The calculations used the optical model parameters of Comfort and Karp [2] and the Love and Franey [12] nucleon-nucleon interaction. This parametrization is sometimes called ''standard'' and will be referred to as such here, and the data will be characterized by comparison with the results of such standard calculations. For the (p,n) calculations the spectroscopic amplitudes are from Cohen, Kurath, and Lee [13,14]. The $^{13}C(p,n)^{13}N$ calculated cross section is the sum of the $\Delta J=0$ and for $\Delta J=1$ cross sections, where ΔJ is the total angular momentum transfer.

Combining the results of the present experiment with previous work [1], it can be seen (Fig. 9) that the $^{12}C(p,p)^{12}C$ cross section has a maximum at about 160° and then decreases out to 180° remaining about 15 times the optical model prediction. Proton elastic scattering from ^{13}C at 200 MeV had previously been measured [15] out to 115°. Over this angular range the situations for ^{12}C and ^{13}C proton elastic scattering are similar in that in both cases the standard calculation follows the data quite closely except that the position of the deepest minimum is predicted to be at too high an angle. The present work shows that near 180° there is again a similarity between the two cases in that the $^{13}C(p,p)$ cross section also decreases towards 180° and is also about an order of magnitude greater than the standard calculation predicts. The fact that the minimum at 180° is deeper for ^{13}C is correctly predicted as is the fact that at this angle the ^{12}C cross sections are about a factor of 2 greater than those for ^{13}C.

The only relevant previous $^{12}C(p,n)^{12}N$ and $^{13}C(p,n)^{13}N$ data are at 160 MeV [16] and cover only forward angles. The results of the standard DWIA calculations at 160 MeV given in Figs. 11 and 12 show that while the calculations qualitatively reproduce the small amount of previously existing data, discrepancies of as much as a factor of 5 appear at

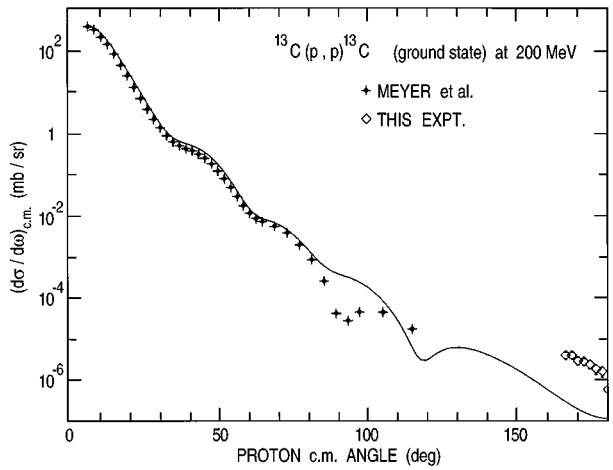

FIG. 10. Prior and present measurements and a DWIA calculation of the $^{13}C(p,p)^{13}C$ elastic scattering differential cross sections at 200 MeV. The crosses are from Ref. [1]. The errors are always smaller that the size of the symbols.

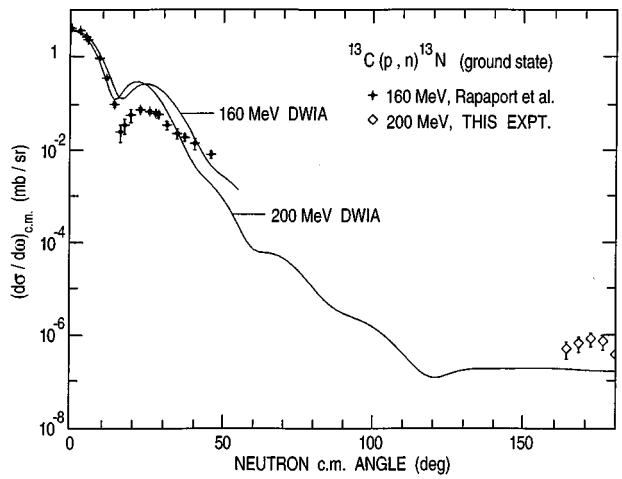

FIG. 12. Prior and present measurements and DWIA calculations of $^{13}C(p,n)^{13}N$ differential cross sections. The crosses are from Ref. [16] at 160 MeV and the diamonds the present work.

TABLE IV. Standard parameters.

V_1 MeV	r_1 fm	a_1 fm	V_2 MeV	r_2 fm	a_2 fm	V_3 MeV	r_3 fm	a_3 fm	V_4 MeV	r_4 fm	a_4 fm
−12.5	1.2	0.68	−13.1	1.2	0.61	−16.4	0.9	0.47	0		

angles as small as about 30°. For both (p,n) reactions the predicted cross sections in the backward direction are about a factor of 5 too small and the observed maximum at about 170° is not reproduced. However, the fact that the cross section of $^{13}C(p,n)$ is about twice that of $^{12}C(p,n)$ is correctly predicted by the standard calculations.

In summary, it is seen that the standard calculations underestimate the cross sections in the 157° to 180° region for all four reactions. For both ^{12}C and ^{13}C the discrepancy for elastic scattering is about a factor of 15 while for (p,n) the calculations are low by about a factor of 5.

III. OPTICAL MODEL CALCULATIONS

A. Sensitivity to the standard potential parameters

The comparison between the near 180° differential cross sections and the standard optical model calculations shows some striking systematics.

(1) In all four cases the calculations reproduce the shape of the angular distribution over the measured region.

(2) For both elastic scattering and the (p,n_0) reaction the ratio of ^{12}C to ^{13}C cross sections is reproduced.

(3) For both elastic scattering and the (p,n_0) reaction the cross sections are underpredicted by about an order of magnitude.

Because this is the first backward angle data for these reactions it is perhaps not surprising that the parameters obtained in previous fits do not lead to an accurate reproduction of the data in this region. For this reason an investigation was made as to which parameters are particularly influential at backward angles and whether these could be altered so as to improve the fit in this region without destroying the agreement at smaller angles. The calculations were performed using the code DW81 [17] which uses a potential of the form

$$U(r)=V_1 f_1(r)+iV_2 f_2(r)+(1/r)[V_3 f_3'(r)+iV_4 f_4'(r)] \times[\vec{L}\cdot\vec{S}]$$

where $f_i(r)=1/[1+\exp(x_i)]$, $x_i=(r-r_i A^{1/3})/a_i$, and $f_i'(r)=df_i(r)/dr$.

Starting with the standard parameters [2], given in Table IV, each parameter was varied in turn in order to see how varying the various parameters affects the angular distribution.

In all of the calculations both the central potential radius and the spin-orbit potential radius were kept at their standard values. When the real central potential depth, V_1, was varied while keeping the other parameters at the standard values it was found that varying the depth does not have a great effect on the cross sections. Even eliminating the real central potential entirely does not completely destroy the fit as can be seen in Fig. 13(a). With V_1 at its standard value of −12.5 MeV reducing the diffuseness of the real central potential, a_1, leads to flatter angular distributions which give a significantly poorer fit to the data, and when a_1 is 0.2 fm or smaller the diffraction pattern becomes more marked [Fig. 13(b)]. However, when the real central depth is reduced to 2 MeV the forward-angle cross sections are insensitive to the diffuseness while the near 180° cross sections are sensitive to a_1 and are well reproduced with $a_1=0.20$ fm [Fig. 13(c) and 13(d)].

For the imaginary central potential no such simple alteration of parameters was found that leads only to an increase in the near 180° cross sections. Varying the imaginary central potential's depth, V_2, does not have much effect until V_2 becomes shallower than ≈5 MeV, whereupon the cross section becomes too large at all angles between about 10° and 120° with little change to the large angle cross sections [Fig. 14(a)]. As a_2 is decreased the angular distribution becomes on the average flatter, and the strong diffraction pattern becomes stronger [Fig. 14(b)].

Decreasing the real spin-orbit potential's depth, V_3, makes the cross section too small at all angles [Fig. 14(c)], and increasing V_3 makes it everywhere too large. Decreasing the diffuseness of this term, a_3, leads to cross sections that are too large at all angles [Fig. 14(d)] while increasing a_3 has the opposite effect.

For $^{13}C(p,p)$ reducing V_1 to −2 MeV and a_1 to 0.2 fm also increases the 180° cross section by about an order to magnitude while having a relatively small effect at the forward angles (Fig. 15). However, substantially reducing V_1 leads to a greatly enhanced (p,n) cross section forward of ≈10°, probably reflecting the fact that the reaction takes place throughout the nuclear volume while the elastic scattering takes place mainly on the surface.

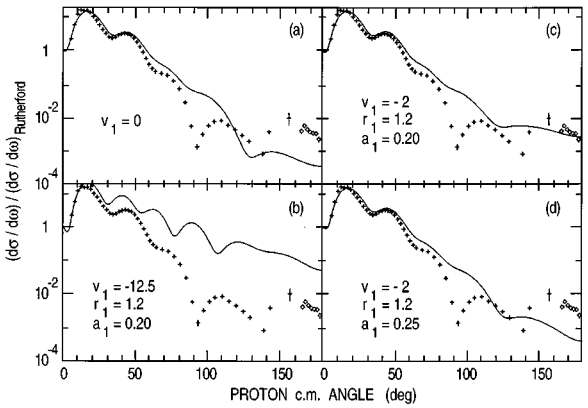

FIG. 13. DWIA calculations of $^{12}C(p,p)$ elastic scattering with various values for the depth and/or the diffuseness of the real central potential and the other parameters those of Ref. [2], or ''standard.''

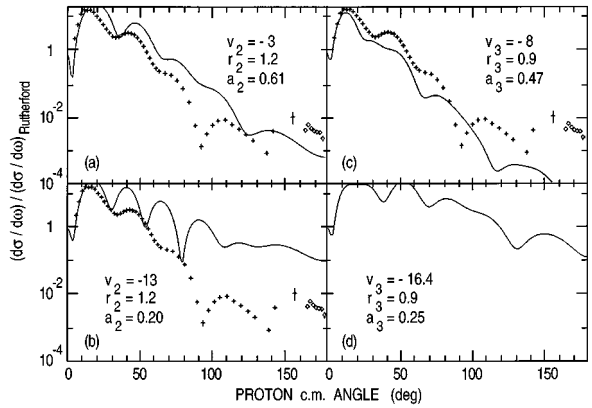

FIG. 14. DWIA calculations of $^{12}C(p,p)$ elastic scattering. The optical potential has the standard parameters except for the imaginary central potential in (a) and (b) and for the real spin-orbit potential in (c) (d).

B. Phenomenological optical model calculation

A phenomenological optical model calculation has been reported [1] which gives a good fit to the differential cross sections out to 130° but falls below the data at larger angles. This calculation uses a relativistically modified Schrödinger equation with relativistic kinematic variables and wave functions and a modified central potential which is the sum of an attractive Woods-Saxon term and a repulsive Woods-Saxon squared term. Because heavy particle exchange is expected to enhance cross sections at large angles, a calculation was performed using the code SNOOPY8Q [18] with the same optical model potentials plus a simple Majorana exchange term in the real central and spin orbit potentials. In the code the potentials were multiplied by $[1+\alpha(-1)^L]$ and $[1+\beta(-1)^L]$ factors for the central and spin-orbit potentials, respectively, where α and β are independently variable strength factors which are chosen phenomenologically. The results obtained with $\alpha=-0.00013$ and $\beta=-0.0001$ are shown in Fig. 16 where it can be seen that the cross sections near 180° are substantially enhanced while those forward of

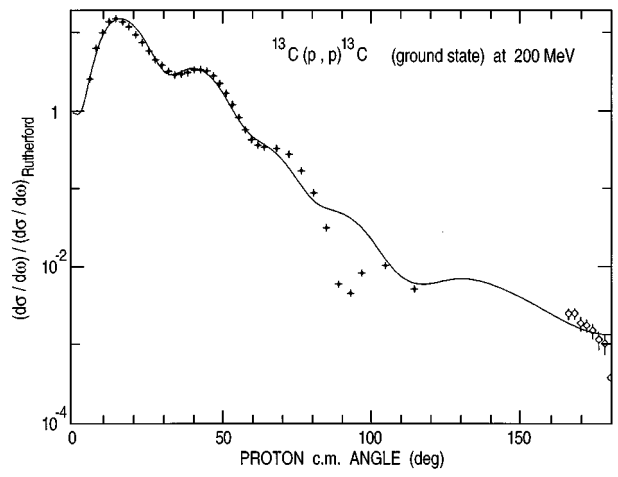

FIG. 15. Experimental data and DWIA calculation of $^{13}C(p,p)$ elastic scattering at 200 MeV using the altered standard parameters ($V_1=-2$ MeV, $a_1=0.2$ fm) that best fit ^{12}C elastic scattering.

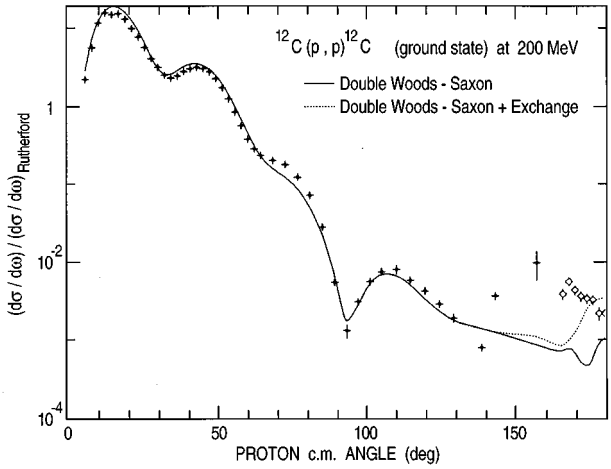

FIG. 16. Experimental data and DWIA calculations of $^{12}C(p,p)$ elastic scattering using a double Woods-Saxon potential as given in Ref. [1] (solid line) and with the addition of a Majorana exchange term (dotted line).

≈140° are not changed. There is also no significant change in the predicted forward angle analyzing powers [1]. However, the 180° peak is much too narrow. Perhaps further modifications of the potentials to reflect high momentum transfer effects or coupling to other channels, such as the 2^+ state at 4.4 MeV, can further improve the fit at large angles.

IV. CONCLUSIONS

This work represents the first measurements of differential cross sections for the $^{12,13}C(p,N)$ reactions at angles greater than 160°. For $^{12}C(p,p)$ the present data combined with that of Ref. [1] gives an angular distribution that goes from 6.7 to 180 degrees. We not only confirm the finding [1] that at large angles the elastic scattering from ^{12}C is larger than predicted by calculations that use the standard optical model parameters but also find that this phenomenon is present in elastic scattering from ^{13}C as well as in both the $^{12}C(p,n)^{12}N$ and the $^{13}C(p,n)^{13}N$ reactions. However, while below 160° the discrepancy between theory and experiment for elastic scattering by ^{12}C increases with increasing angle [1], the present work shows that the cross section reaches a maximum at about 160° and that the ratio of calculation to experiment remains roughly constant out to 180°. For the other reactions, the data below 180° is much less complete but in the 160°–180° region all four reactions show approximately the same discrepancy between calculation and experiment. For elastic scattering the near 180° cross sections can be reproduced by altering the real central potential so that it is much shallower and has a less diffuse surface and when this is done, the fit gets somewhat worse at the more forward angles. However, a much shallower real central potential leads to much too large (p,n) cross sections at all but the most forward angles. Adding an exchange term to a double Woods-Saxon potential enhances the cross section at 180° while not harming the good fits to the previously reported [1] data below 130°, but the enhancement is a narrow peak at 180° rather than the observed broad maximum centered at about 160°. It thus appears likely that a new form of the potential will have to be introduced in order to explain the large angle (p,N) cross sections.

[1] H. O. Meyer, P. Schwandt, W. W. Jacobs, and J. R. Hall, Phys. Rev. C **27**, 459 (1983).
[2] J. R. Comfort and B. C. Karp, Phys. Rev. C **21**, 2162 (1980).
[3] J. Homolka, W. Schott, W. Wagner, W. Wilhelm, R. D. Bent, M. Fatyga, R. E. Pollock, M. Saber, R. E. Segel, P. Kienle, and K. E. Rehm, Nucl. Instrum. Methods A **260**, 418 (1987); J. Homolka, Ph.D. thesis, Technische Universität, München, 1989.
[4] M. A. Green, Ph.D. thesis, Indiana University IUCF Internal Report 83-3a, 1983.
[5] Program MINUIT, CERN Program Library Writeup D506.
[6] W. Schott, W. Wagner, P. Kienle, R. Pollock, R. Bent, M. Fatyga, J. Kehayias, M. Green, and K. Rehm, Phys. Rev. C **34**, 1406 (1986); J. Homolka, W. Schott, W. Wagner, W. Wilhelm, R. D. Bent, M. Fatyga, R. E. Pollock, M. Saber, R. E. Segel, and P. Kienle, *ibid*. **38**, 2686 (1988); **45**, 1276 (1992).
[7] Written by H. Ernst, Argonne National Laboratory (1981); modified by K. Lesko, Argonne National Laboratory (1984).
[8] J. B. Marion and F. C. Young, *Nuclear Reaction Analysis: Graphs and Tables* (North-Holland, Amsterdam, 1968).
[9] Y. Baudinet-Robinet, Nucl. Instrum. Methods **190**, 197 (1982); Phys. Rev. A **26**, 62 (1982).
[10] K. Shima, N. Kuno, and M. Yamanouchi, Phys. Rev. A **40**, 3557 (1989); At. Data Nucl. Data Tables **51**, 173 (1981).
[11] Z. Yu, Ph.D. thesis, Northwestern University, 1993.
[12] W. G. Love and M. A. Franey, Phys. Rev. C **24**, 1073 (1981); **31**, 488 (1985).
[13] S. Cohen and D. Kurath, Nucl. Phys. **A73**, 1 (1965); **A101**, 1 (1967).
[14] T.-S. H. Lee and D. Kurath, Phys. Rev. C **21**, 293 (1980).
[15] H. O. Meyer, P. Schwandt, G. L. Moake, and P. P. Singh, Phys. Rev. C **23**, 616 (1981).
[16] J. Rapaport, T. Taddeucci, C. Gaarde, C. D. Goodman, C. C. Foster, C. A. Goulding, D. Horen, E. Sugarbaker, T. G. Masterson, and D. Lind, Phys. Rev. C **24**, 335 (1981).
[17] Program DWBA70 by R. Schaeffer and J. Raynal (unpublished); extended by J. R. Comfort (unpublished code DW81); modified by C. Olmer (unpublished).
[18] P. Schwandt, Indiana University Cyclotron Facility Report No. 84-2, 1984.